

This item is an archived official version of:

"Demonstration of photonic temperature sensor for RTM-6 composite manufacturing process (180°C) integrated with PMOC system"

By Georgios Syriopoulos, Aggelos Poulimenos, Giannis Pouloupoulos, Maria Poulimenou, Jeroen Missinne, Michal Szaj, Charalampos Zervos, Geert Van Steenberge, Hercules Avramopoulos.

doi: 10.1117/12.2649992

And is made available with permission, based on the SPIE Web Posting Policy, as explained on:
<https://www.spiedigitallibrary.org/article-sharing-policies>

Copyright 2023 Society of Photo-Optical Instrumentation Engineers (SPIE). One print or electronic copy may be made for personal use only. Systematic reproduction and distribution, duplication of any material in this publication for a fee or for commercial purposes, and modification of the contents of the publication are prohibited.

To refer to or to cite this work, please use the citation to the published version:

Georgios Syriopoulos, Aggelos Poulimenos, Giannis Pouloupoulos, Maria Poulimenou, Jeroen Missinne, Michal Szaj, Charalampos Zervos, Geert Van Steenberge, Hercules Avramopoulos, " Demonstration of photonic temperature sensor for RTM-6 composite manufacturing process (180°C) integrated with PMOC system," Proc. SPIE 12424, Integrated Optics: Devices, Materials, and Technologies XXVII, 1242416 (17 March 2023); doi: 10.1117/12.2649992.

PROCEEDINGS OF SPIE

SPIDigitalLibrary.org/conference-proceedings-of-spie

Demonstration of photonic temperature sensor for RTM-6 composite manufacturing process (180°C) integrated with PMOC system

Georgios Syriopoulos, Aggelos Poulimenos, Giannis Pouloupoulos, Maria Poulimenou, Jeroen Missinne, et al.

Georgios Syriopoulos, Aggelos Poulimenos, Giannis Pouloupoulos, Maria Poulimenou, Jeroen Missinne, Michal Szaj, Charalampos Zervos, Geert Van Steenberge, Hercules Avramopoulos, "Demonstration of photonic temperature sensor for RTM-6 composite manufacturing process (180°C) integrated with PMOC system," Proc. SPIE 12424, Integrated Optics: Devices, Materials, and Technologies XXVII, 1242416 (17 March 2023); doi: 10.1117/12.2649992

SPIE.

Event: SPIE OPTO, 2023, San Francisco, California, United States

Demonstration of photonic temperature sensor for RTM-6 composite manufacturing process (180°C) integrated with PMOC system

Giorgos Syriopoulos^a, Aggelos Poulimenos^b, Giannis Pouloupoulos^a, Maria Poulimenou^b, Jeroen Missinne^c, Michal Szaj^d, Charalampos Zervos^a, Geert Van Steenberge^c, Hercules Avramopoulos^a

^aPhotonics Communications Research Laboratory National Technical University of Athens, Greece;

^bEngineering Technology Solutions E.E. Athens, Greece;

^cCenter for Microsystem Technology (CMST) Ghent University and IMEC Ghent, Belgium;

^dArgotech a.s. Trutnov, Czech Republic;

ABSTRACT

We demonstrate a sensing platform for composite manufacturing (RTM-6) process based on silicon photonics, being controlled by novel Process Monitoring Optimization Control (PMOC) system. The photonic multi-sensor is based on Bragg grating components, allowing measurements of temperature, pressure and refractive index, and is packaged employing a ball lens fiber-to-chip interface. We present results of the packaged temperature photonic sensor regarding bandwidth, linearity and thermo-optic efficiency, being controlled by our PMOC system. We experimentally achieve 0.074 nm/C with $R^2 = 0.995$ linearity for temperature up to 180°C (RTM-6 compatible) with 1 kHz data acquisition and 0.2°C accuracy.

Keywords: Photonic temperature sensor, composite material fabrication, Bragg grating, process monitoring and control, miniaturized multi sensor, composite molds, silicon photonics

INTRODUCTION

Composite materials have seen wide adoption in several sectors, owing mainly to their high strength, low weight, high stiffness and thermal stability. Those characteristics have made them ideal replacements of metal alloys in the aerospace industry. The use of autoclaves can assure the production of high-quality parts, with significant costs, not only because of the high initial investments required, but also of the excessive energy consumption of the method itself. The adoption of out-of-autoclave processes, such as the Resin Transfer Molding (RTM) method, which uses metallic and, recently, composite tools, can address those concerns, though the trade-off with the quality of the manufactured part persists[1]. Better monitoring of the process during several filling and curing cycles, can increase the quality of the produced parts and ensure repeatability.

To achieve this, different solutions are already available, with thermocouples and capacitance sensors as prime examples. However, those thermoelectric solutions suffer in terms of size since the mechanical characteristics of the parts can be dramatically altered by the embedding of sensors. The most important issue though, lies in the electrical conductivity of the composite components themselves, when carbon fibres are used[2]. This necessitates the use of integrated photonic sensors, due to their small footprint, low cost and immunity to electromagnetic interference, that will measure key parameters for the optimization of the manufacturing procedure.

CONCEPT

The production of the composite parts relies on cycles of heating and cooling in tightly controlled conditions of pressure and vacuum. The sensors that will be described allow the monitoring of the resin's flow and the curing procedure. The multisensor is a series of Bragg grating structures implemented in a Silicon Photonics platform and is embedded in the composite mold using Through Thickness Reinforcement techniques. The schematic of a donut-shaped multisensor can be seen in Figure 1. To achieve direct contact with the resin, the sensors are fabricated on top of the Photonic Integrated

Circuit (PIC). This will allow for a more accurate measurement of the temperature, pressure at various points and of the resin’s refractive index, as it changes during the curing process. For compatibility with established practices in the aerospace industry, an interrogator is used, so a single fiber is needed, which is coupled on the bottom side of the chip. The

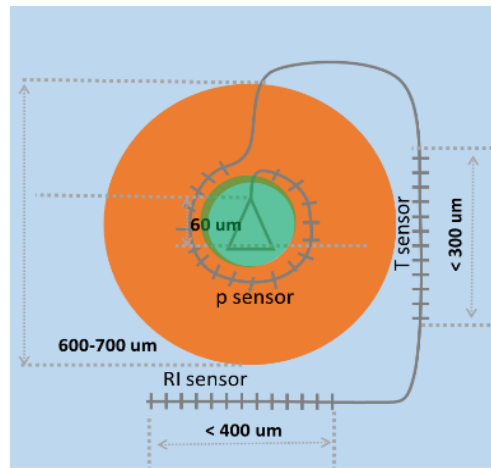


Figure 1 The top view of a multisensor with a grating coupler at the center

performance requirements for the temperature sensor include a dynamic range starting from room temperature, up to 200 °C and a resolution of 0.2 °C.

PMOC OPERATIONAL PRINCIPLE AND SPECIFICATIONS

The aim of the Process Monitoring Optimization and Control (PMOC) system is to collect the photonic (PIC) sensor data along with other available field data and subsequently exploit the acquired information for performing a series of process

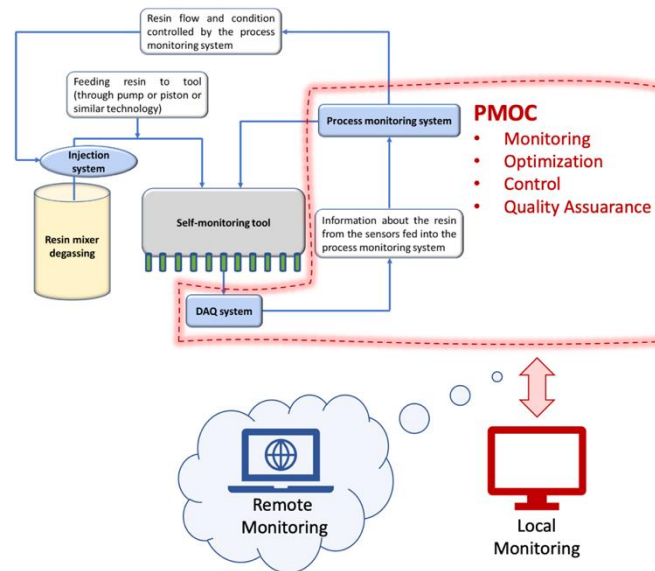


Figure 2 Schematic diagram of the PMOC system operational principle

control, optimization and Quality Assurance operations. At the same time, the PMOC system will be able to provide process

monitoring information in a local and remote manner. The PMOC system was developed in the context of the SEER project, as outlined in Figure 2. The prototype PMOC system has two entities: (a) the hardware unit and (b) the software for its operation. The PMOC hardware unit performs the Data Acquisition (DAQ) operations, implements the processing activities and produces the required outputs for the control of the self-monitoring tool, while the PMOC software provides a Graphical User Interface (GUI) for the local and remote monitoring of the whole manufacturing process. The detailed PMOC system functionalities and hardware/software specifications are presented in Table 1 and Table 2.

Table 1: Summary of the PMOC system functionalities.

PMOC system functions			
Process Monitoring (PM)	Process Optimization & Control (POC)	Quality Assurance (QA)	Tool Monitoring (TM)
<ul style="list-style-type: none"> • PIC raw data monitoring. • PIC temperature, pressure and refractive index monitoring • Thermocouple temperature monitoring. • Virtual Sensor temperature monitoring. 	<ul style="list-style-type: none"> • Tool temperature control. • Part temperature control (virtual sensor based). • Cure process control 	<ul style="list-style-type: none"> • Quality Assurance indices extraction. 	<ul style="list-style-type: none"> • Tool performance monitoring. • Tool integrity monitoring (temperature based).

Table 2: Summary of the PMOC system hardware specifications.

PMOC system specifications: Data Acquisition hardware		
Optical Interrogator	Thermocouple	Pulse Width Modulation (PWM)
<ul style="list-style-type: none"> • Number of channels: 16 • Update rate: 2 Hz • Processing unit communication: Ethernet. 	<ul style="list-style-type: none"> • Number of channels: 16. • Update rate: 2 Hz. • Processing unit communication: USB, ethernet, embedded. 	<ul style="list-style-type: none"> • Number of input channels: 16. • Number of output channels: 16. • Update rate: 1 KHz. • Embedded signal processing.
PMOC system specifications: Processing and control hardware		
Processing Unit	Control loop	Power electronics
<ul style="list-style-type: none"> • Processing speed (functions update period): 500 msec. • DAQ H/W communication: Ethernet. • User interface communication: Ethernet, local display port. 	<ul style="list-style-type: none"> • Multizone heating control. • Up to 16 heating zones. • Control period: 500 msec. • Power electronics control: Pulse Width Modulated (PWM) signal. 	<ul style="list-style-type: none"> • Independent power regulation for each heating zone. • Up to 16 heating zones. • Heating power: Up to 5A per heating zone. • Pulse Width Modulated (PWM) control signal.

PMOC system specifications: Monitoring and user interface hardware	
Local monitoring	Remote monitoring
<ul style="list-style-type: none"> • Display H/W: Local Monitor. • User input H/W: Local keyboard/mouse. • Embedded Processing H/W unit H/W communication 	<ul style="list-style-type: none"> • Laptop PC. • Processing unit H/W communication: Ethernet

The PMOC system design consists of 3 interconnected levels:

1. The Field Programmable Gate Array (FPGA) level, which is responsible for the implementation of the data acquisition and signal generation operations using National Instrument FPGA hardware.
2. The real-time processing level, which performs all the necessary real-time signal processing, decision making and data handling/storage operations along with the hosting of the local process monitoring User Interface. The real-time processing level is based on the National Instrument CompactRIO platform[3].
3. The windows monitoring level, which offers remote (through ethernet) process monitoring, process data access and post processing capabilities.

The developed prototype PMOC system and some indicative PMOC User Interface screenshots, are depicted in Figure 3.

TEMPERATURE SENSOR DESIGN

The surface relief Bragg gratings sensors are based on a 220 nm Silicon platform, with a sidewall variation along the propagation axis. The design takes place in two phases. The first is a study of the guided modes, in which we will calculate the effective refractive index for the TE, TM polarization. The material layer stack as well as the field intensity for different

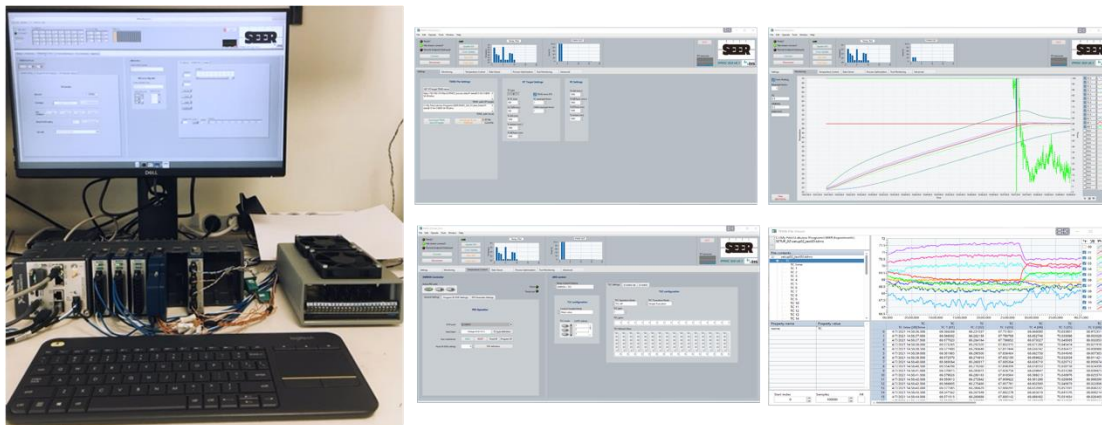


Figure 3: The Process Monitoring Optimization and Control (PMOC) prototype system, developed for SEER.

modes is shown in Figure 2. Since a silicon integration platform is used, the values for the refractive index are 3.47 for silicon waveguide, 1.45 for Buried Oxide (BOX), and 1.41 for the top cladding layer. As the resonance wavelength for each of the Bragg structures is located around 1550 nm, it will be possible to determine the grating pitch (Λ), for different variations of the corrugation width (dw), based on the expression:

$$\lambda_B = 2 \cdot n_{eff} \cdot \Lambda$$

It should be noted that the filling factor (FF) is 50%. The topview as well as the design variables are shown in Figure 4.

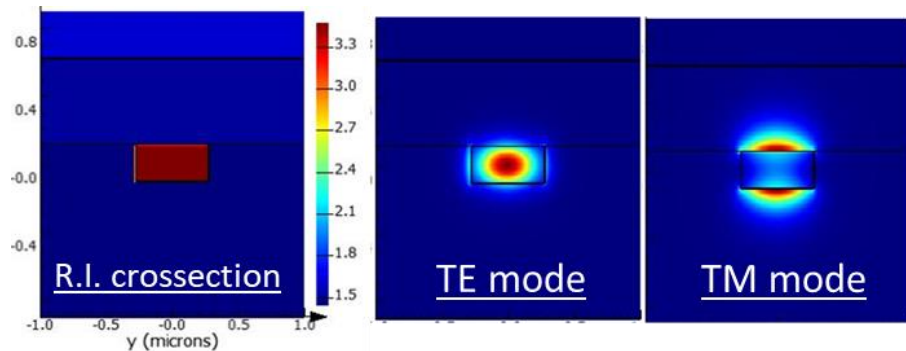


Figure 4 The layer stack (left) and the field intensity for every polarization (right)

Different design choices for the polarization will influence the multisensor performance accordingly. With a TE polarization, the field intensity is concentrated on the silicon channel, making it more sensitive during temperature changes, and immune to the change of the refractive index and pressure field during the curing process. By adopting a TM polarization, we get the opposite effect, owing to the profile of the E/M field.

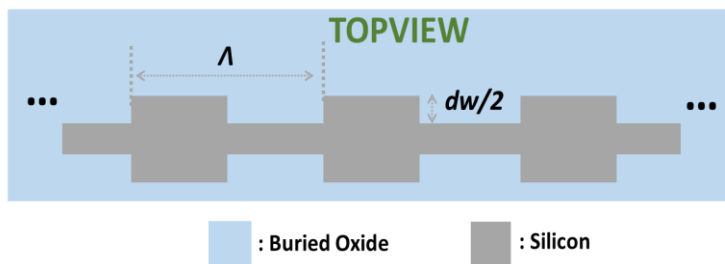


Figure 5 The top view of the grating structure

With a suitable selection of a range of values for the pitch and the corrugation width, the power in the propagation direction will be studied, and the spectral response will be tailored to minimize the insertion losses and the bandwidth of the main reflection lobe. To calculate the spectrum of the reflections, the EigenMode Expansion (EME) solver will be used, found

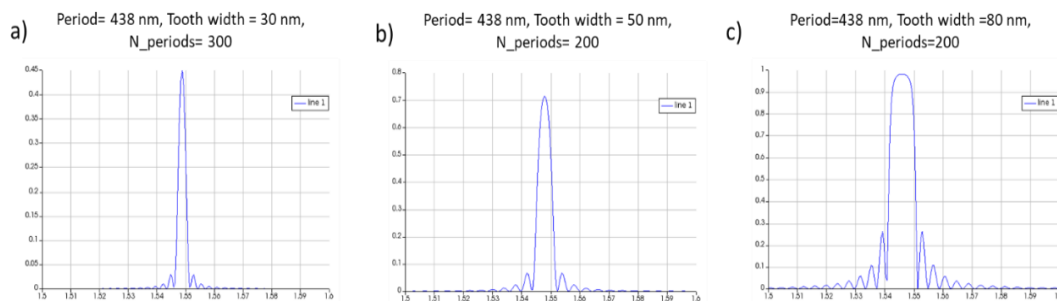


Figure 6 Spectral response of Bragg grating structures

in commercial software by Lumerical. This algorithm uses the scattering matrix method to model periodic waveguide discontinuities[4]. For a better-defined central wavelength, phase shifted Bragg gratings are also investigated, which can provide a steep dip in the reflection spectrum. Some indicative results for different Bragg grating structures can be seen in

As we saw before, the grating pitch affects only the Bragg resonance. By varying the width of the sidewall corrugation, the insertion losses and the lobe bandwidth is influenced. With an increase in the total number of periods, the optical filter has a higher spectral selectivity.

Below, in Figure 7, we show simulation results for various phase shifted Bragg gratings, with a constant corrugation width. They consist of two identical gratings with a single unperturbed period in the middle. This configuration results in a Lorentzian dip in the reflection, which will help in a more accurate definition of the resonance wavelength during the experimental validation. [5]

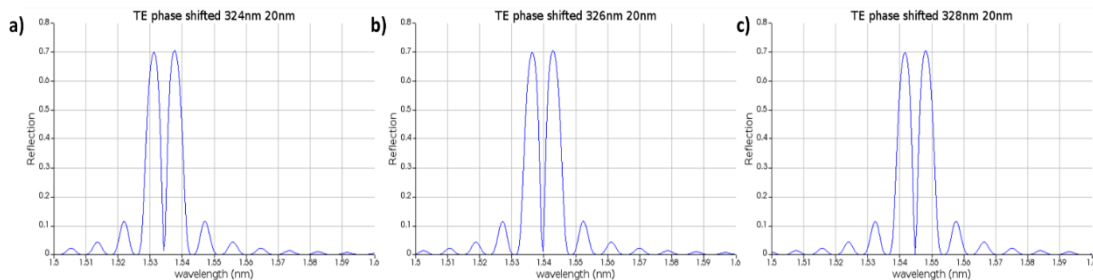


Figure 7 Spectral response of phase shifted Bragg grating structures for varying Λ

As in the previous periodic structures, we can notice that with an increase in the grating pitch, the Bragg resonance wavelength increases. Repeating the process shown previously, the next step is to simulate the variation of corrugation width for the phase-shifted gratings. Observing Figure 8, which consists of the reflection spectra for $\Lambda = 328$ nm and with increasing corrugation width, we conclude that the maximum of the reflection spectrum is increased, and the bandwidth of the main lobe is reduced.

After concluding the simulations with the temperature regarded as constant, the design process continues considering the temperature variation, according to RTM requirements. The thermo-optic effect that is modelled, causes a change in the

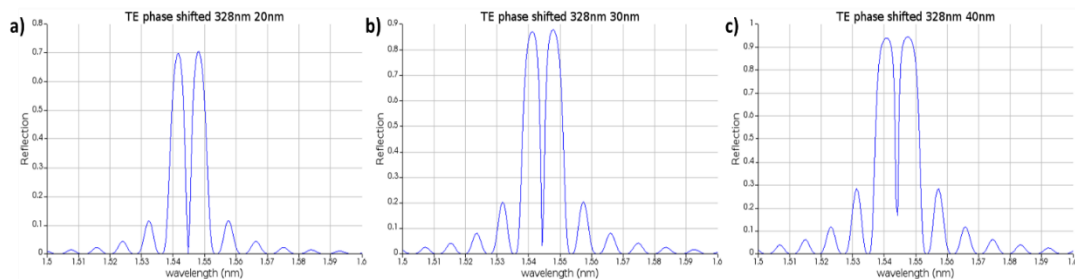


Figure 8 Spectral response of phase shifted Bragg grating structures for varying dw

refractive index in all materials, with the highest effect taking place in silicon, with a thermo-optic coefficient of $\frac{dn}{dT} = 18 \times 10^{-5} \text{ K}^{-1}$ in the C-band. The Bragg structures' thermal sensitivity can be given by the expression:

$$\frac{d\lambda}{dT} = \frac{\lambda}{n_g} \frac{dn_{eff}}{dn} \frac{dn}{dT}$$

Simulations modelling the thermo-optic effect are executed using again the EME algorithm, with built-in thermo-optic models for all materials, for a temperature range starting from 27 °C up to 187 °C. For a TE polarization temperature sensor, the spectrum of the Bragg reflections as well as the shift of the central wavelength for both types of polarizations are shown in Figure 9. As the temperature rises, silicon expands, increasing the grating pitch and so, the resonance wavelength. The effect on the resonance wavelength is shown to be linear, with a thermo-optic tuning efficiency of 0.070 nm/°C and 0.044 nm/°C for TE and TM polarization mode.

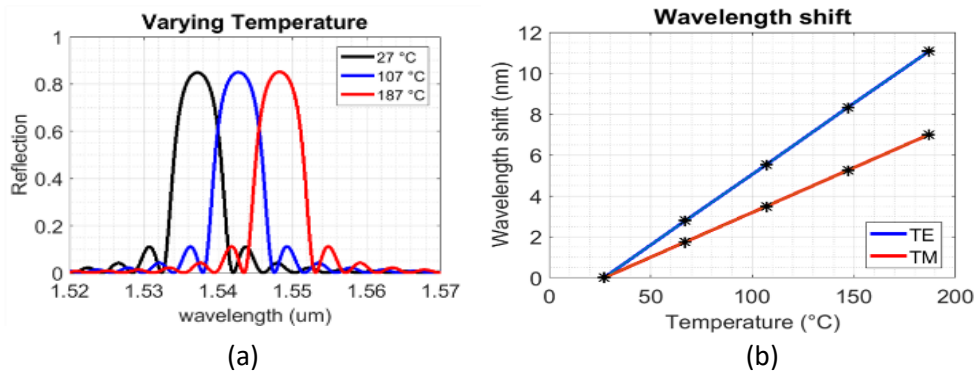


Figure 9 The reflection spectrum (a) and central wavelength (b) shift

The packaged chip employs a ball lens fiber-to-chip interface with a metal fixture used to place a ceramic ferrule, the fiber that it contains and the silicon chip. The ball lens couples the light through the back side of the PIC, requires polishing of the substrate and is placed inside the metal fixture and is glued with epoxy resin. The coupling between the PIC and the fibre is optimized by aligning the ceramic ferrule with the silicon chip and curing the epoxy resin used to keep it fixed. The packaged optical sensor is inserted into a metal rod, for mechanical and thermal stability and protection during the embedding process and allows for a sensor configuration with an overall diameter of less than 2 mm. Parts of the packaging can be seen in Figure 10 as well as the silicon chip located on top.

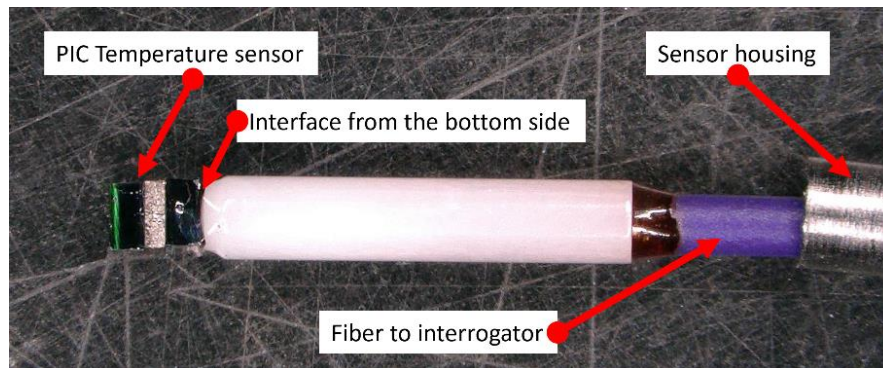


Figure 10 The packaged sensor configuration

TESTBED AND RESULTS

For the characterization of the sensors, we use a commercially available interrogator, that includes a tunable laser source, with TE or TM polarization operation. It can cover a bandwidth up to 39.2 nm in the C-band, with a frequency of 2 kHz. It also measures the reflection spectrum, making it possible to define the Bragg resonance, and thus, the gratings' characteristics, though it gives us relative values of the measured power[6]. Since the shift caused by the change in temperature is deemed as critical, the instrument's characteristics are not considered limiting.

The testing of the photonic sensors was accomplished using the PMOC system described in previous Subsection. The prototype system that was used during the temperature measurement experiments is shown in Figure 11.



Figure 11 Photonic temperature sensor measurement using the PMOC system

The PMOC system consists of the real-time processing unit shown in Figure 11, which hosts the User Interface for local monitoring/ system control purposes and communicates through ethernet with the photonic interrogator.

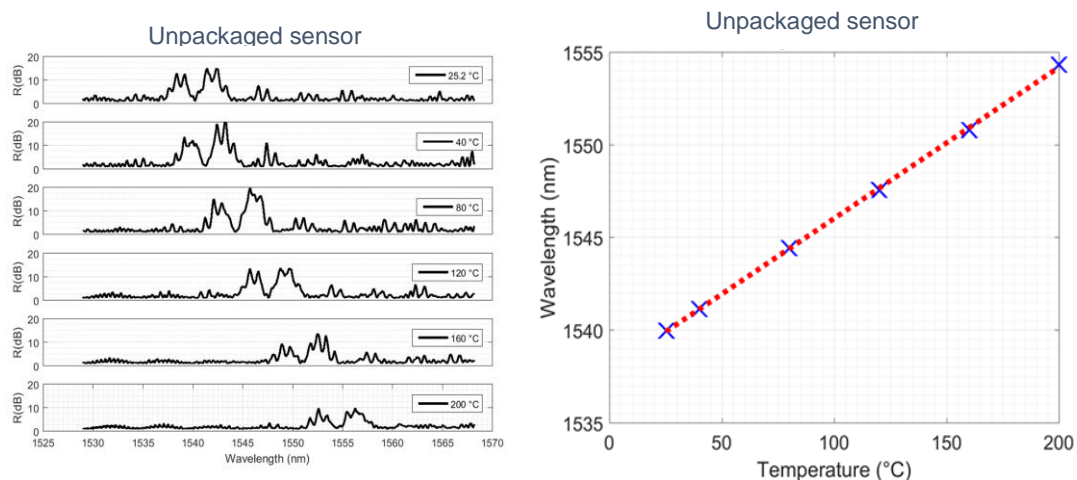


Figure 12 Reflection spectrum (left) and linear fitting (right) of the central wavelength for an unpackaged phase shifted sensor

For the packaged chips characterization, most of the optical components of the experimental testbed presented in previous sensor iterations can be made redundant [7], so a single polarization controller (PC) is used, a single SMF fiber to couple the interrogator to the PC, as well as the heat block containing the Pt100 temperature sensor with an accuracy of 0.1°C.

We can see in Figure 12 the spectrum and the central wavelength of the reflections from an unpackaged phase shifted Bragg sensor. A red-shift in the spectrum can be noticed during a temperature increase up to 200°C, with a mean value of thermo-optic tuning efficiency of 0.0825 nm/°C is measured, with significant linearity ($R^2 = 0.99967$).

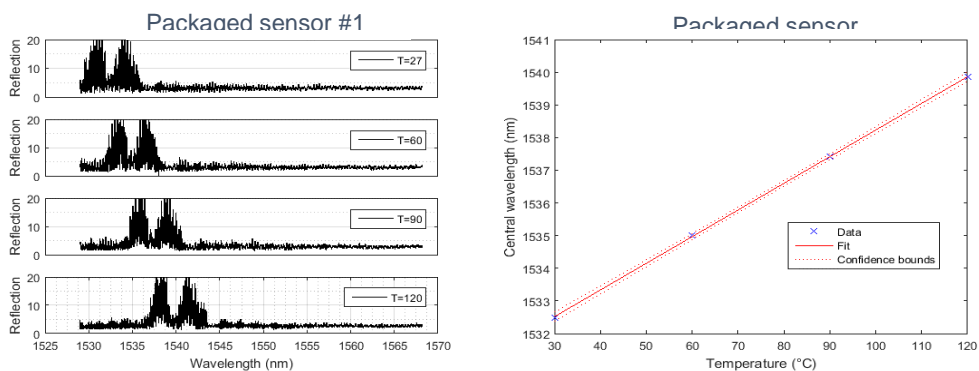


Figure 13 Reflection spectrum (left) and linear fitting (right) of the central wavelength for TE sensor #1

Figure 13 presents the reflection spectrum for a TE packaged sensor, with a central wavelength at 1532 nm at room temperature. We can observe a linear response to the variation of temperature, with a very high R^2 , and a thermo-optic tuning efficiency of 0.081 nm/°C, close to the one expected.

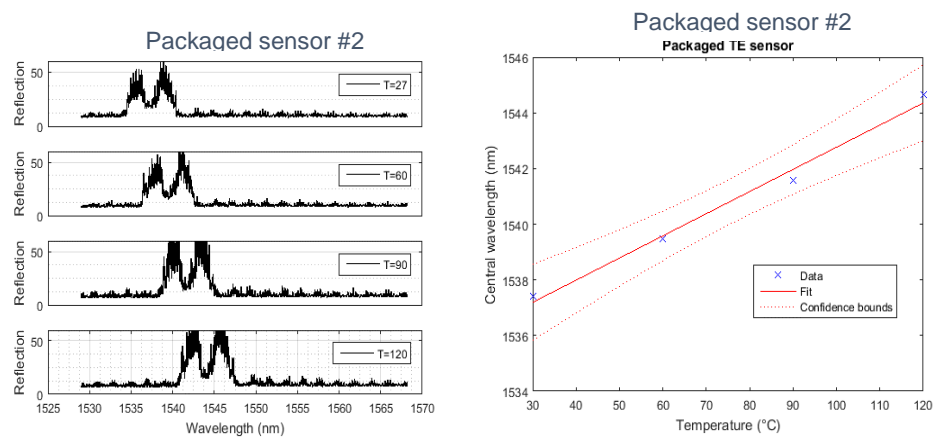


Figure 14 Reflection spectrum (left) and linear fitting (right) of the central wavelength for TE sensor #2

Figure 14 shows the reflection spectrum for a second TE packaged sensor, with a central wavelength at around 1537 nm at room temperature. Again, high linearity is observed with varied temperature ($R^2 = 0.99$), and a thermo-optic sensitivity of 0.079 nm/°C, close to the highest predicted from the design.

CONCLUSIONS

We presented a novel temperature sensor based on Bragg gratings and fabricated on a silicon photonics platform. The design process of Bragg structures was discussed, for both TE and TM polarization operation. The experimental testbed was presented, as well as the characterization for the TE sensors that were fabricated. Their response to the variation of temperature is shown, and a sensitivity of ≈ 0.080 nm/°C is measured, with high linearity. The high thermo-optic tuning efficiency is explained from the strong confinement of light in the silicon core, with a TE polarization operation.

ACKNOWLEDGEMENTS

This work has received funding from the European Union's Horizon 2020 innovation program under grant agreement No. 871875 (SEER).

REFERENCES

- [1] O. A. Ekuase, N. Anjum, V. O. Eze, and O. I. Okoli, 'A Review on the Out-of-Autoclave Process for Composite Manufacturing', *J. Compos. Sci.*, vol. 6, no. 6, p. 172, Jun. 2022, doi: 10.3390/jcs6060172.
- [2] K. Tifkitsis and A. Skordos, 'A novel dielectric sensor for process monitoring of carbon fibre composites manufacture', *Compos. Part Appl. Sci. Manuf.*, vol. 123, pp. 180–189, Aug. 2019, doi: 10.1016/j.compositesa.2019.05.014.
- [3] 'https://www.ni.com/en-lb/shop/compactrio.html'.
- [4] D. F. G. Gallagher and T. P. Felici, 'Eigenmode expansion methods for simulation of optical propagation in photonics: pros and cons', presented at the Integrated Optoelectronics Devices, San Jose, CA, Jun. 2003, p. 69. doi: 10.1117/12.473173.
- [5] G. P. Agrawal and S. Radic, 'Phase-shifted fiber Bragg gratings and their application for wavelength demultiplexing', *IEEE Photonics Technol. Lett.*, vol. 6, no. 8, pp. 995–997, Aug. 1994, doi: 10.1109/68.313074.

- [6] S. K. Ibrahim, M. Farnan, D. M. Karabacak, and J. M. Singer, 'Enabling technologies for fiber optic sensing', presented at the SPIE Photonics Europe, Brussels, Belgium, Apr. 2016, p. 98990Z. doi: 10.1117/12.2234975.
- [7] I. Pouloupoulos, C. Zervos, G. Syriopoulos, J. Missinne, M. Szaj, and H. Avramopoulos, 'Silicon photonics temperature and refractive index sensor for curing process monitoring in composite material industry', in *Optical Sensing and Detection VII*, May 2022, vol. 12139, pp. 76–88. doi: 10.1117/12.2621285.